

Quantum Butterfly Effect at the Crossroads of Spontaneous Symmetry Breaking

Pranaya Pratik Das* and Biplab Ganguli†

Department of Physics and Astronomy, National Institute of Technology Rourkela, Odisha-769008, India

(Dated: April 28, 2023)

In classical mechanics, spontaneous symmetry breaking of the Hamiltonian can embroil the dynamics of some regular systems into chaos. The classical and quantum pictures are not entirely different in these broken symmetric regions. There exists a correspondence between them, but for a brief time window. However, our numerical observations show that quantum mechanics can emulate the opposite role and forge exponential fluctuations in classically non-chaotic systems within an early-time window by introducing a symmetry-breaking term to the Hamiltonian. In this work, we have taken four one-dimensional quantum mechanical models: two Inverted Harmonic Oscillators(IHOs), a triple Well and IHO with a plateau. Then we spontaneously break the already existing symmetry in their Hamiltonian with varying perturbation strength to bring anomaly into the system. Then, we use numerical diagnostic tools such as OTOC, Loschmidt echo and spectral form factor(SFF) to detect the anomalies that may sweep into the system with the introduction of the asymmetry. Our primary focus is on the behaviour of OTOC as it reduces to the Lyapunov exponent in the classical limit, and we observe exponential growth, as expected. However, these exponential growths of OTOC are not widespread over the entire potential well but are limited only to the eigenstates in the neighbourhood of the broken symmetry. These results suggest that the exponential growth of OTOC, backed by Loschmidt echo and SFF, is due to asymmetry. In other words, OTOC detects the effect of symmetry-breaking, which is often synonymous with the butterfly effect.

Keywords: Symmetry breaking, OTOC, Loschmidt Echo, IHO, SFF, Chaos, Quantum Chaos

CONTENTS

I. Introduction	1
A. OTOC	2
B. Loschmidt Echo	3
C. Outline	4
II. Models	4
A. IHOs	4
B. <i>Model(III)</i> : Triple Well	6
C. <i>Model(III)</i> : IOH with a plateau	7
III. Numerical Observations	7
OTOC	8
1. Model(I)	8
2. Model(II)	9
3. Model(III)	11
4. Model(IV)	12
IV. Discussion	12
Loschmidt Echo	14
Spectral Form Factor	15
V. Conclusion	15
References	16

I. INTRODUCTION

In some Hamiltonian systems, introducing a small symmetry-breaking term can serve as perturbation and drags these systems out of symmetric states into asymmetric ones. Here, most of the phase space persists in behaving as if symmetries still exist, except in the regions where the symmetry-breaking term allows resonance to occur, ultimately leading to chaos in the neighbourhoods of these nonlinear resonances. This phenomenon of spontaneous symmetry breaking leading to

* pranaya.phy@outlook.com

† biplabg@nitrkl.ac.in

chaos is highly evident in classical systems, usually characterised by hypersensitivity to perturbations in initial conditions under the Hamiltonian evolution. We can reconfirm this most common characteristic of chaotic systems by studying individual orbits in phase space. However, due to the Heisenberg uncertainty principle, the volume occupied by a single quantum state in the classical phase space is \hbar^N for a system with N degrees of freedom. Hence, we no longer have the luxury of following individual orbits. This necessitates the need for a new chaos diagnostic tool for quantum systems. There are many such tools discovered, as shown in Fig.(1)[1]. One such tool, initially considered in the context of superconductivity but rapidly gaining traction in the high energy and condensed matter communities, is the Out-of-Time-Order Correlator(OTOC).

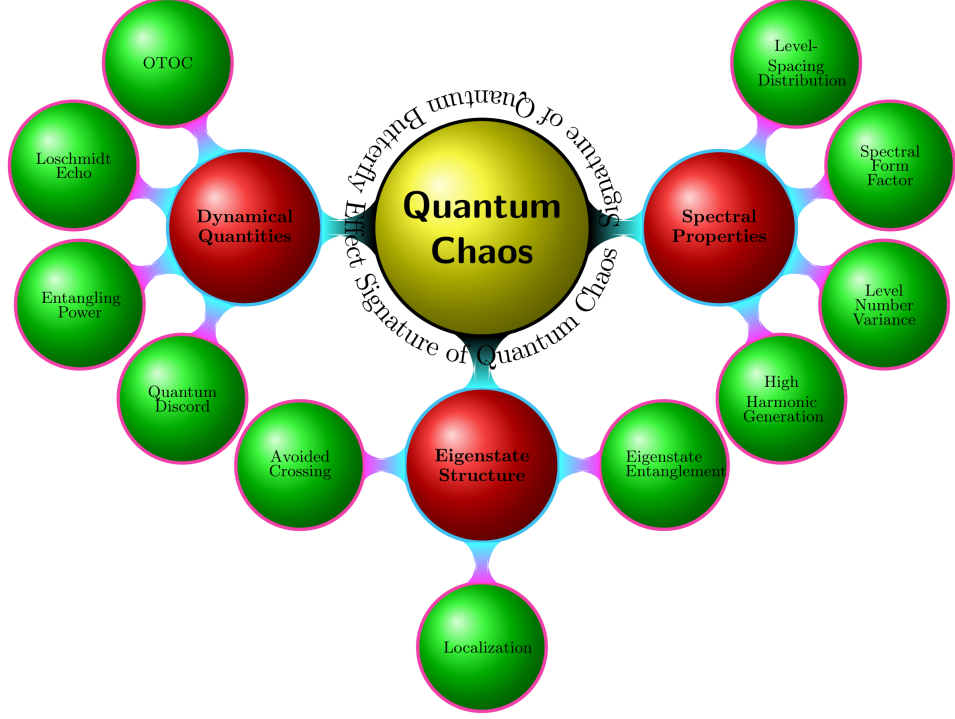


FIG. 1. Classification of signatures of quantum chaos and their diagnostic tools.

A. OTOC

The OTOCs, within the framework of quantum mechanics, are the growth of non-commuting quantum mechanical operators describing the Unequal Time Commutation Relations (UTCRs). It is the most potent quantum mechanical analogue of the classical sensitivity to the initial conditions. However, the OTOC measures sensitivity quite differently compared to its classical counterpart. Firstly, OTOC can measure a more nuanced notion of sensitivity as quantum corrections allow it to contain higher-order derivatives of $x(t)$. Secondly, the quantum terms are dominant at the *scrambling time* (*Ehrenfest time*)¹, which explains known deviations from exponential growth at this early time scale, as shown in Fig.(2(b)).

We consider the four-point OTOC defined by

$$\mathcal{C}_\beta(t) = -\left\langle [\hat{x}(t), \hat{p}]^2 \right\rangle \quad (1)$$

where, $\beta = \frac{1}{k_B T}$, also known as “the coldness function”, \hat{x} and \hat{p} are respectively quantum mechanical operators for position and momentum.

Using the classical-quantum correspondence, $\frac{[\cdot]}{i\hbar} \rightarrow \{\cdot, \cdot\}$, one can show its subtle relation with the classical Lyapunov exponent as follows,

$$\begin{aligned} \frac{1}{i\hbar} \langle [x(t), p(0)] \rangle &\rightarrow \{x(t), p(0)\} = \frac{\partial x(t)}{\partial x(0)} \sim e^{\lambda_L t} \\ -\frac{1}{\hbar^2} \langle [x(t), p(0)]^2 \rangle &\rightarrow \{x(t), p(0)\}^2 = \left(\frac{\partial x(t)}{\partial x(0)} \right)^2 \sim e^{2\lambda_L t} \end{aligned} \quad (2)$$

¹ The Ehrenfest time, $t_E \sim \frac{1}{\lambda_L} \ln\left(\frac{k_\beta}{\hbar}\right)$, where λ_L is the Lyapunov exponent.

This gives the classical diagnostic of the butterfly effect, i.e., the exponential dependence of the final position on small changes in the initial position. Thus, from the above semi-classical connection, we may say OTOC quantifies the sensitive dependence on the initial condition of the time evolutions for both chaotic and non-chaotic systems in quantum mechanics.

For a natural Hamiltonian with the form,

$$\mathcal{H} = \sum_{i=1}^N \frac{p_i^2}{2} + \mathcal{U}(x_1, x_2, \dots, x_N), \quad (3)$$

and partition function,

$$Z(\beta) = \sum e^{-\beta \mathcal{H}} = \sum_m e^{-\beta E_m} \quad (4)$$

Eq.(1) can take the form as given in [2–4], i.e.

$$\mathcal{C}_\beta(t) = \frac{1}{Z(\beta)} \sum_m e^{-\beta E_m} c_m(t) \quad (5)$$

where, $H |m\rangle = E_m |m\rangle$ and

$$c_m(t) = \frac{1}{4} \sum_{k,l,r} x_{ml} x_{lk} x_{rm} x_{kr} \left(E_{rk} E_{lk} e^{it E_{rl}} + E_{mr} E_{ml} e^{-it E_{rl}} - E_{rk} E_{ml} e^{it(E_{rm} + E_{lk})} - E_{mr} E_{lk} e^{-it(E_{rm} + E_{lk})} \right) \quad (6)$$

We shall refer $c_m(t)$, in Eq.(6), for a fixed energy eigenstate as *Microcanonical OTOC* and $\mathcal{C}_\beta(t)$, in Eq.(5), as a *Thermal OTOC*. Here, $E_{nm} = E_n - E_m$, $x_{nm} = \langle n | \hat{x} | m \rangle$ and $p_{nm} = \langle n | \hat{p} | m \rangle$.

[3, 5] showed that OTOC could give false flags of chaos in the presence of a local maximum. Here, we take the help of symmetry breaking by varying a parameter present in the system potential until the local maximum ceases to exist. In this scenario, OTOC still shows exponential growth even when there is no local maximum present in the system. We reconfirmed our findings by taking different models and later measuring Loschmidt Echo and Spectral Form Factor(SFF) under similar scenarios.

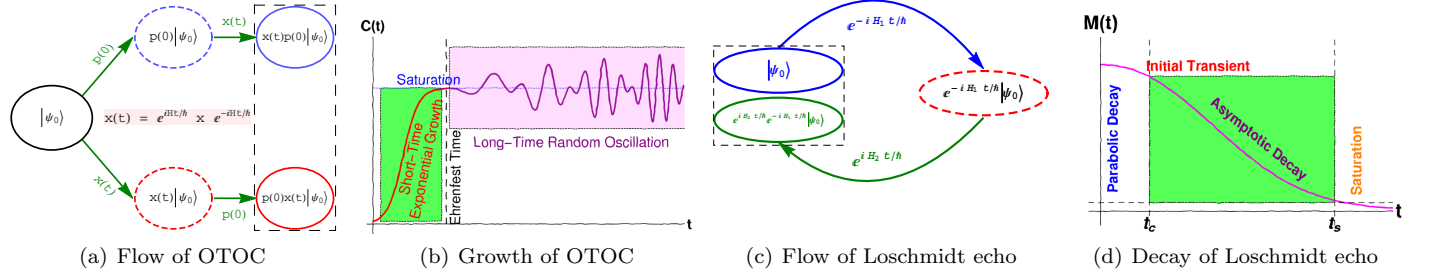


FIG. 2. (a) Shows a schematic flow of a four point OTOC, (b) shows typical time-dependence of the OTOC for one-body and finite-size many-body systems exhibiting different behaviour in the short and long-time regimes, (c) shows a schematic flow Loschmidt Echo, (d) shows decay of Loschmidt echo in a quantum systems with chaotic classical limit.

B. Loschmidt Echo

The Loschmidt echo measures the revival occurring under an imperfect time-reversal procedure applied to a complex quantum system. This tool quantifies the sensitivity of quantum evolution to isospectral perturbations². Any spectral quantity will remain unaffected, but the Loschmidt echo will generally decay, Fig.(2(d)).

Mathematically, the Loschmidt echo is then defined as,

$$M(t) = |A(t)|^2 = \left| \langle \Psi_0 | e^{i\hat{\mathcal{H}}_2 t/\hbar} e^{-i\hat{\mathcal{H}}_1 t/\hbar} | \Psi_0 \rangle \right|^2 \quad (7)$$

where $A(t)$ is the Loschmidt amplitude. It quantifies the “distance” (in the Hilbert space) between the state $e^{-i\hat{\mathcal{H}}_1 t} |\psi_0\rangle$, resulting from the initial state $|\psi_0\rangle$ in the course of evolution through a time t under the Hamiltonian \mathcal{H}_1 , and the state

² No change in the spectrum of the unperturbed Hamiltonian

$e^{-i\hat{\mathcal{H}}_2 t} |\psi_0\rangle$ obtained by evolving the same initial state through the same time t , but under a slightly different perturbed Hamiltonian \mathcal{H}_2 as shown in Fig.(2(c)). The LE, by construction, equals unity for $t = 0$ and typically decays further in time.

Perfect recovery of $|\psi_0\rangle$ would be achieved by choosing $\mathcal{H}_2 = \mathcal{H}_1$, which leads to $M(t) = 1$, but this is an impossible task in realistic problems and $M(t)$ is usually a decreasing function in t . The notion of time reversal i.e. a backward time evolution from t to 0 under \mathcal{H}_2 is equivalent to the forward evolution between t and $2t$ under the Hamiltonian $-\mathcal{H}_2$.

C. Outline

This paper is organised as follows. In section(II), we consider the Hamiltonian form of an *Inverted Harmonic Oscillator(IHO)* and devise three models, namely *Model(I)* and *Model(II)*. Then we construct two more models, *Model(III)* and *Model(IV)*, which are a *triple well* and an *Modified IHO*, respectively. In this section, we solve the Schrödinger equations of these quantum mechanical models under different perturbation strengths and show the energy distributions. By adding perturbation, we break the primitive symmetry present in these systems and force them to devolve into asymmetric states. In section(III), we measure the effect of symmetry breaking by measuring microcanonical and thermal OTOCs. Section(IV) contains a detailed analysis of our numerical observations containing Loschmidt echo in section(IV), and SFF in Section(IV). Finally, in section(V), we summarise our results and make a few closing remarks.

II. MODELS

The harmonic oscillator Hamiltonian is given by,

$$H = \frac{\hat{p}^2}{2m} + \frac{m\omega^2}{2}\hat{x}^2 \quad (8)$$

Here, we work in the natural units($\hbar = 1$) and, without any loss of generality, we assume that the mass of the oscillator, $m = 1$. Depending on the value of frequency ω , three different cases arises: for real positive value, we have a harmonic oscillator potential, for zero, we have a free particle and for imaginary number, we have an inverted harmonic oscillator(IHO)[6]. In this work, we will be mainly concerned with the Hamiltonian of the inverted harmonic oscillator.

Classically, the inverted oscillator has an unstable point in phase space at ($x= 0, p= 0$); a particle accelerates exponentially away from the fixed point when perturbed. Hence, its solutions to Newton equations diverge exponentially in phase space, a characteristic of chaotic motion. It is worth noting that the inverted quantum oscillator is not just a toy model; it has been realized experimentally [7–9] and has even played a role in mathematics, in attacking the Riemann hypothesis [10]. It also provides important insights into the bound of the Lyapunov exponents [11].

A. IHOs

Let us consider, a Hamiltonian of the system without perturbation:

$$\hat{\mathcal{H}} = \frac{-1}{2}\nabla_x^2 + \hat{V}(x) \quad (9)$$

here, we regard \hat{V} as a local approximation of some Hermitian operators, such as:

$$\hat{V}(x) = a_0\hat{x}^4 - a_2\hat{x}^2 - \eta \quad (10)$$

where, a_0 , a_1 and η are constants parameters.

Obviously, $\hat{\mathcal{H}}$ in Eq.(9) is an approximation of \hat{H} in Eq.(8) in the limit $x \rightarrow 0$. The x^4 term is included for the system to be bounded from below. Otherwise, the system would not have any ground state and defining temperature(T) would have been impossible. Based on the values of a_0 and a_2 , we have considered two IHO models; *Model(I)* and *Model(II)*. Note that the parameter a_2 determines the curvature of the unstable top of the hill, a_0 determines the width of the wells, and η ensures that the minimum potential lies on the x-axis. The values of η for different perturbation strength is given in table(I).

$$Model(I) \rightarrow \left\{ a_0 = \frac{1}{50}, a_2 = 0.64 \right.$$

&

$$Model(II) \rightarrow \left\{ a_0 = \frac{1}{128}, a_2 = \frac{1}{4} \right.$$

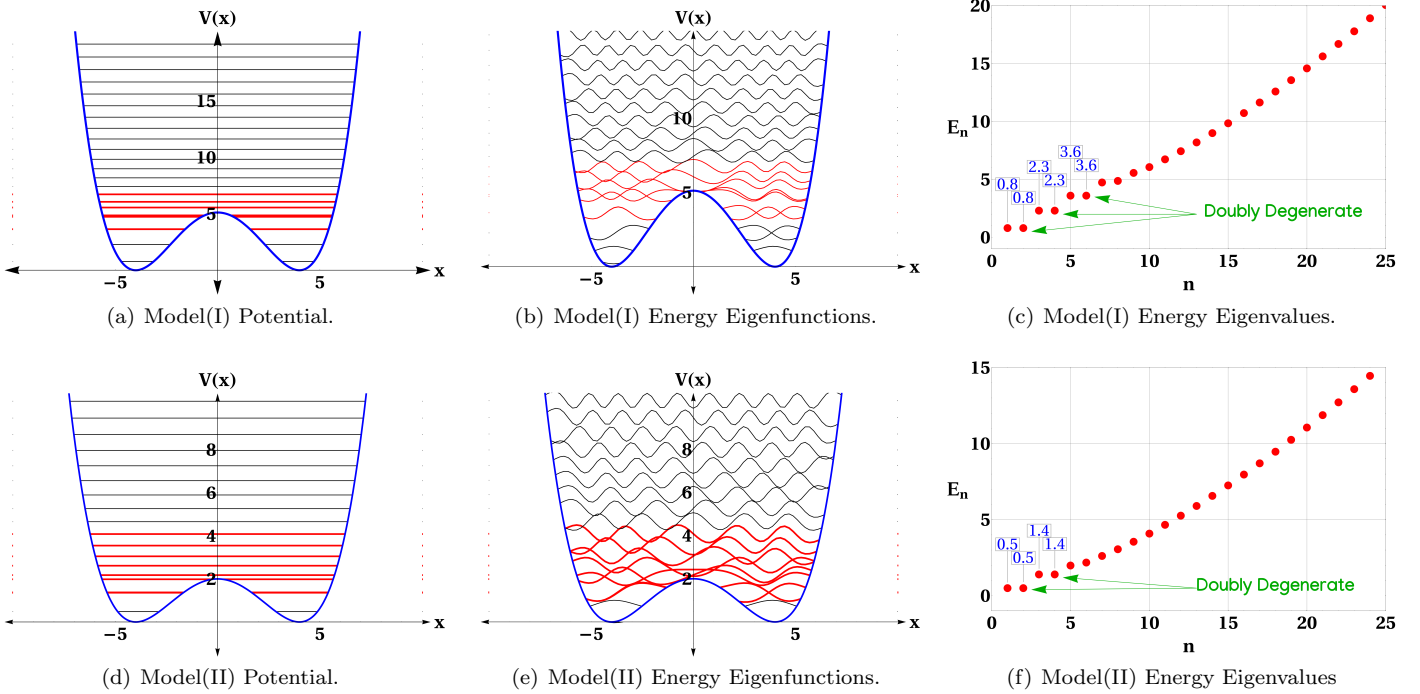


FIG. 3. Potential shape and energy eigenvalues of IHO potentials. The energy levels below the top of the hill are doubly degenerated, and the red lines near the hilltop of the potential show exponential growth in OTOC.

TABLE I. Values of η for different values of asymmetry parameter(σ).

σ	η			
	Model(I)	Model(II)	Model(III)	Model(IV)
0.0	-5.1200	-2.0000	-0.0061	-10.082
0.15	-5.0450	-1.9250	-0.1578	-10.1686
10.0	-10.3949	-7.6240	-10.3587	-15.9209
30.0	-22.2524	-21.3750	-32.5009	-
50.0	-	-	-	-40.3437
70.0	-49.6698	-55.0179	-	-

We numerically solve Eq.(8) in *Mathematica 12.0* on *Ubuntu 20.04 LTS* platform using *NDEigensystem* built-in command and obtain the energy eigenvalues E_n , and the wave functions $\psi_n(x)$ for all the models. The results are shown in Fig.(3). All our numerical observations on these two models are done by considering the width (ΔL) to be 20, ranging from -10 to 10. Below $\Delta L = 15$, the energy separation between levels proliferates, causing the calculation of thermal OTOC very challenging.

As explained in [12], “degeneracies are far more likely to occur for Hamiltonian systems with symmetries than those without symmetries”. It is very likely to be seen here as the degenerate eigenstates begin to split with the addition of a perturbation which breaks the symmetry of the system, forming an asymmetric potential well. The Hamiltonian for the asymmetric double-well potential with perturbation becomes,

$$\hat{\mathcal{H}} = \frac{-1}{2} \nabla_x^2 + V(x) + \sigma \sqrt{\frac{a_0}{2a_2}} \hat{x} \quad (11)$$

where, the parameter σ is equal to shift between the bottoms of the wells which is otherwise known as the asymmetric parameter (distance between the dashed lines in the Fig.(4) and Fig.(5)). It is obvious that, in this constructed system, non-degenerate energy doublets have a splitting $\Delta = \sigma$, i.e. splitting between levels remains close to σ for all doublets lying below the barrier top. The initial inspiration for devising the model is taken from [13–16].

We define *effective asymmetric parameter* in the following way:

$$\sigma = \sqrt{\frac{a_2}{2a_0}} \frac{(\nu\epsilon)}{\pi} \quad (12)$$

where, ϵ and ν are perturbation strength and frequency of perturbation respectively, and $\epsilon\nu$ is known as the *perturbation parameter*.

IHO is a one-dimensional Hamiltonian system, hence its classical analogous system is regular. But this does not mean that the Lyapunov exponent vanishes. The system is unstable around $x = 0$, so we have a non-vanishing classical Lyapunov exponent saddle there.

We quantize the system and consider the time-independent Schrödinger equation as given in Eq.(10) as

$$-\frac{d^2\psi}{dx^2} + \left[a_0 \hat{x}^4 - a_2 \hat{x}^2 - \eta \right] \psi + \left[\sigma \sqrt{\frac{a_0}{2a_2}} \hat{x} \right] \psi = E\psi \quad (13)$$

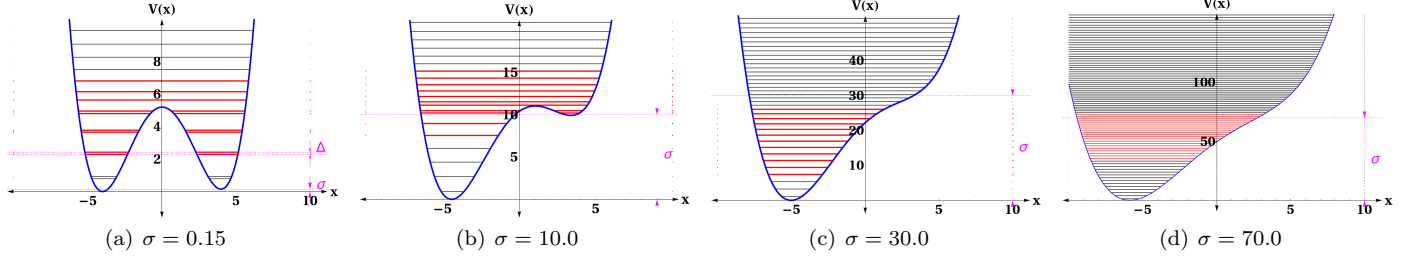


FIG. 4. *Model(I)* with different values of σ .

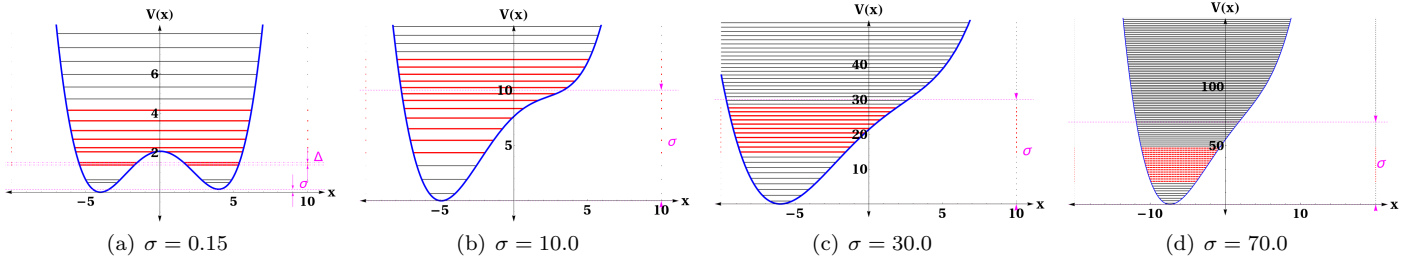


FIG. 5. *Model(II)* with different values of σ .

We numerically solve this equation and obtain the energy eigenvalues E_n and the wave functions $\psi_n(x)$. In Fig.(4) and Fig.(5), we show the obtained distribution of the energy eigenvalues of inverted harmonic oscillators for σ having values 0.15, 10.0, 30.0 and 70.0 for *Model(I)* and *Model(II)*.

B. *Model(III) : Triple Well*

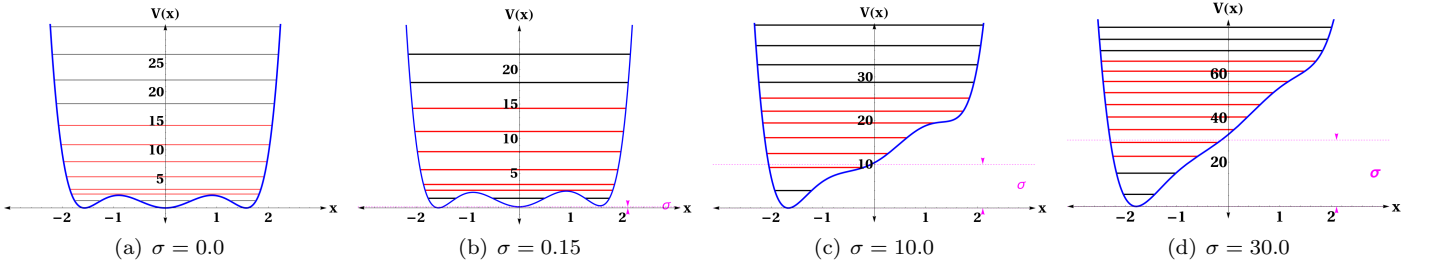


FIG. 6. *Model(III)* with different values of σ .

Triple-well potentials have applications in various areas of physics, such as in the study of molecular dynamics, where they can be used to model the behaviour of molecules in a triple-well potential energy landscape. They also have possible applications in quantum computing, where they can be used as a building block for quantum gates and algorithms.

This model is primarily inspired by the work on [6, 17, 18]. The Hamiltonian of the triple well system is

$$H = \frac{p^2}{2m} + \left[a_2 x^2 - a_0 x^4 + x^6 - \eta \right] + \sigma \sqrt{\frac{a_0}{2a_2}} x \quad (14)$$

where $m = 1$, $a_0 = 4.9$, $a_2 = 6$.

We quantize Eq.(14) and numerically solve the time-independent Schrödinger equation for different values of σ as given in Eq.(15). Fig.(6) shows the potential structure and the corresponding energy eigenvalue distributions under different values of σ having values: 0.0, 0.15, 3.0 and 10.0.

$$-\frac{d^2\psi}{dx^2} + \left[a_2 \hat{x}^2 - a_0 \hat{x}^4 + \hat{x}^6 - \eta \right] \psi + \left[\sigma \sqrt{\frac{a_0}{2a_2}} \hat{x} \right] \psi = E\psi \quad (15)$$

C. Model(III) : IOH with a plateau

The Hamiltonian for this asymmetric double-well potential[19, 20] with perturbation has a modified version of the potential give in Eq.(10):

$$V(x) = a_0 \hat{x}^6 - a_2 \hat{x}^4 - \eta \quad (16)$$

where $a_0 = \frac{1}{142}$, $a_2 = 0.15$, x^4 produces a plateau instead of a hilltop and x^6 term gives a lower bound to the potential. The values of η can be obtained from the table(1).

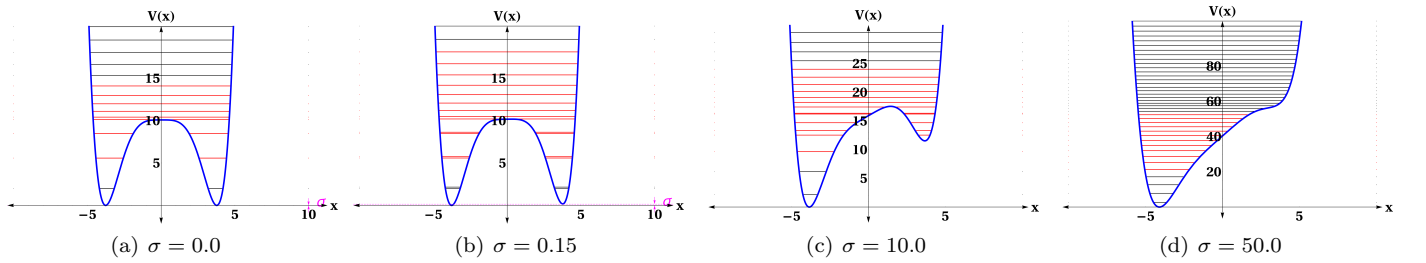


FIG. 7. Model(IV) with different values of σ .

The double-well potential arises in various contexts in physics, including in the study of condensed matter systems, such as in modelling phase transitions and superconductors' behaviour. It is also used in quantum mechanics to model the behaviour of a particle in a symmetric potential energy landscape. The energy barrier between the two wells in *Model(I)* and *Model(II)* is relatively low and narrow. However, in this model, barrier is broader and taller for which quantum particles are more likely to become trapped in one of the wells.

III. NUMERICAL OBSERVATIONS

As mentioned in [3], Fig.(8(a)) and Fig.(8(c)) show that the exponential growth of microcanonical OTOC for both *Model(I)* and *Model(II)* respectively. This exponential growth of OTOC falls under a small window of energy levels around the hilltop of the potential, portrayed in red. Similarly, for higher temperatures, the thermal OTOC shows exponential growth shown in Fig.(8(b)) and Fig.(8(d)) respectively for *Model(I)* and *Model(II)*.

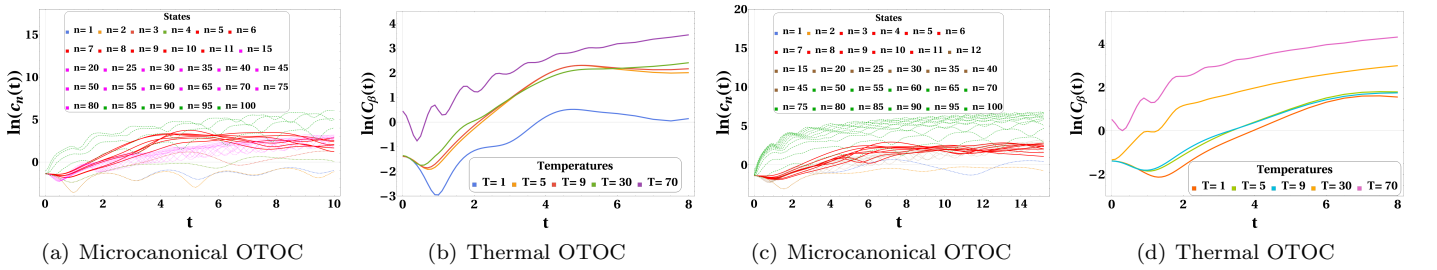
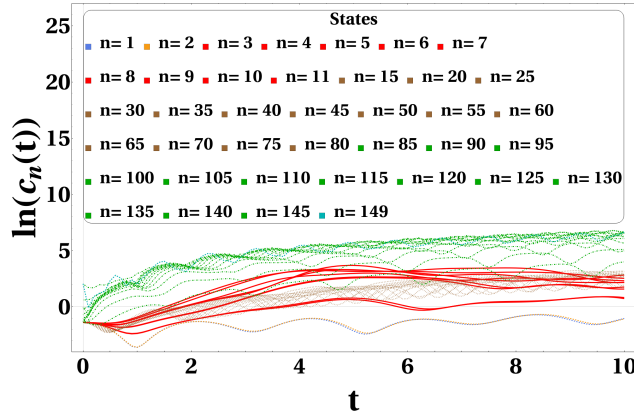


FIG. 8. OTOCs for *Model(I)* are shown in (a) & (b). And for *Model(II)*, the same is shown in (c) & (d), respectively for $\sigma = 0.0$.

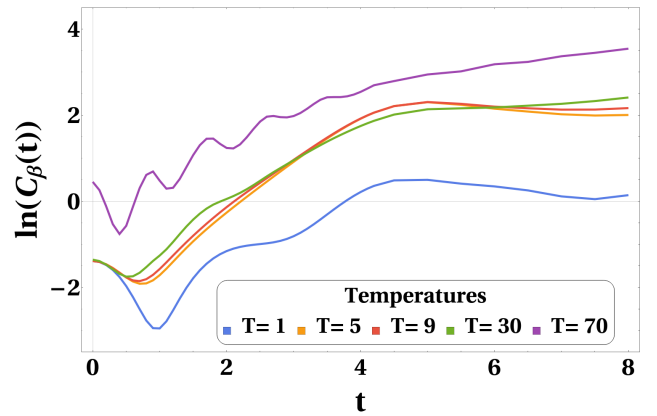
In this section, we numerically observe the behaviours of OTOC by adding a small symmetry-breaking term into the system potential. In other words, we measure the effect of the perturbation on the behaviour of OTOC. Further We have discussed the results from Loschmidt echo and Spectral Form Factor(SFF) on these models.

1. Model(I)

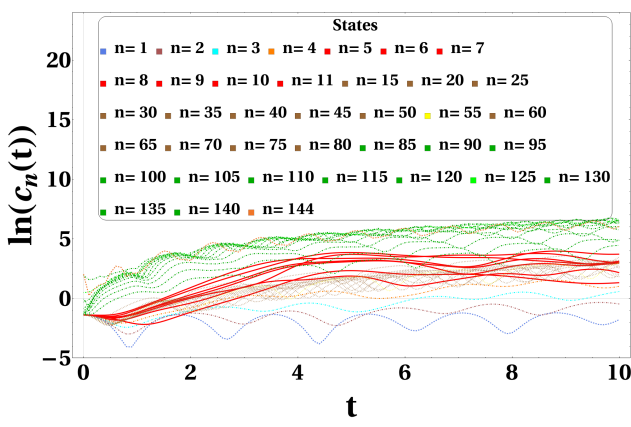
Here, we have numerically evaluated Eq.(6) and Eq.(5) for Thermal and microcanonical OTOCs respectively for different strength of asymmetry parameter(σ). Fig.(9), Fig.(10), Fig.(11) and Fig.(12) shows the behaviour of OTOCs for σ having values 0.15, 10, 30 and 70, respectively.



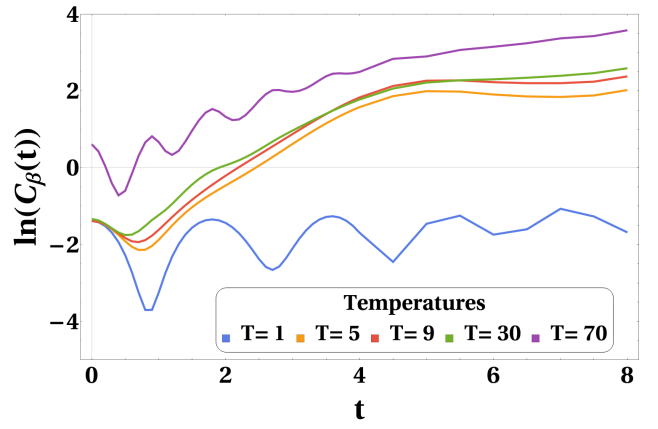
(a) Microcanonical OTOC



(b) Thermal OTOC

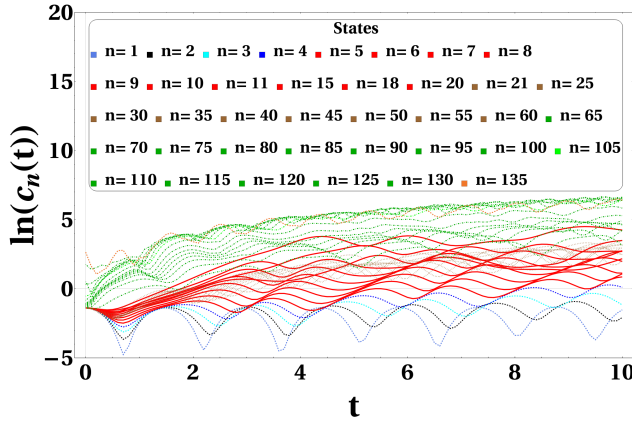
FIG. 9. OTOCs of Model(I) with $\sigma = 0.15$.

(a) Microcanonical OTOC

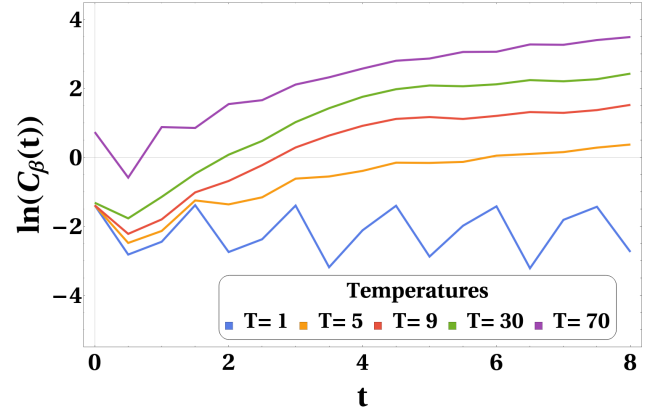


(b) Thermal OTOC

FIG. 10. OTOCs of Model(I) with $\sigma = 10.0$.

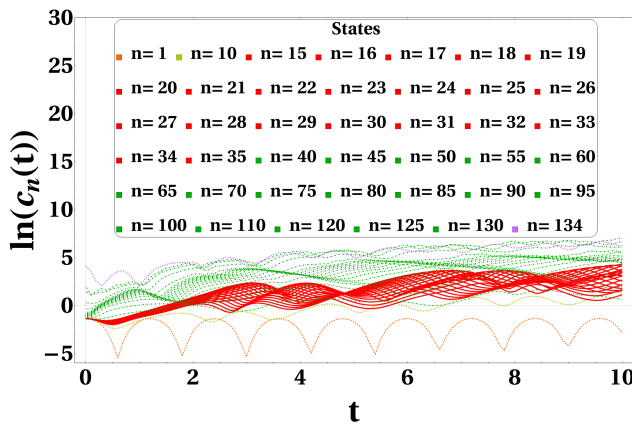


(a) Microcanonical OTOC

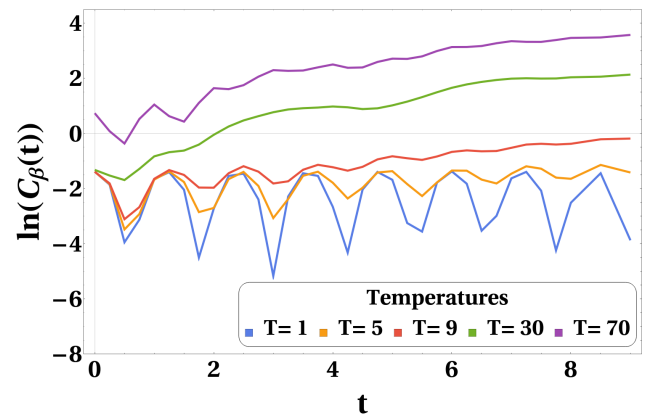


(b) Thermal OTOC

FIG. 11. OTOCs for *Model(I)* with $\sigma = 30.0$.



(a) Microcanonical OTOC



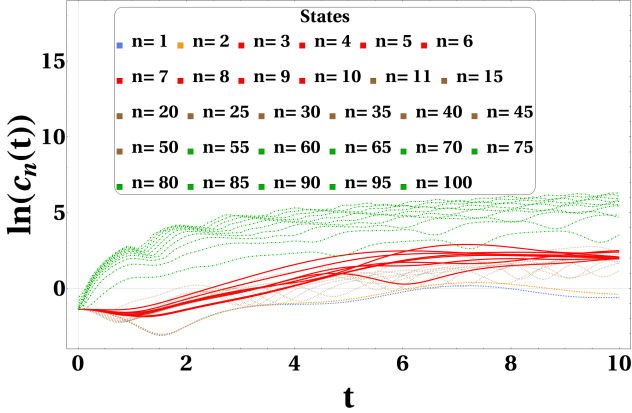
(b) Thermal OTOC

FIG. 12. OTOCs for *Model(I)* with $\sigma = 70.0$.

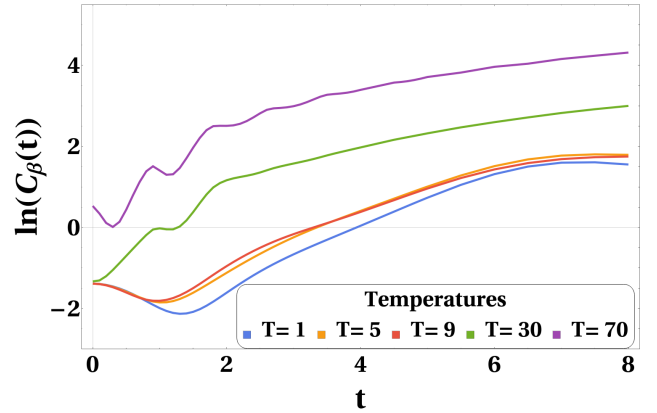
In Fig.(9) and Fig.(10), we find exponential growth of OTOCs around the hilltop of the potential for $\sigma = 0.15$ and 10, respectively as verified previously. While in Fig.(4(c)), for $\sigma = 30.0$, the local maximum starts to disappear from the potential but, both microcanonical and thermal OTOCs continues to show exponential growth as we can find in Fig.(11). For $\sigma = 70$, in Fig.(4(d)), the local maximum is completely absent in the potential, but we can still find exponential growth for a very narrow band of energy levels in Fig.(12). Here, the time duration of exponential growth is very small compared to the rest.

2. *Model(II)*

Here, again for Model(II), we numerically evaluated Eq.(6) and Eq.(5) for the same strength of asymmetry parameter(σ) as mentioned in Table(I). Fig.(13), Fig.(14), Fig.(15) and Fig.(16) shows the behaviour of OTOCs for σ having values 0.15, 10, 30 and 70, respectively.

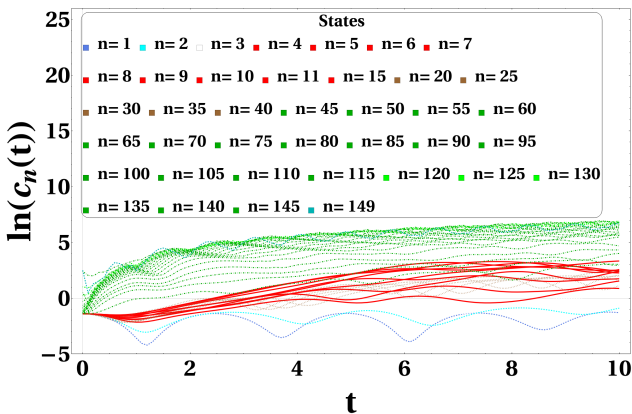


(a) Microcanonical OTOC

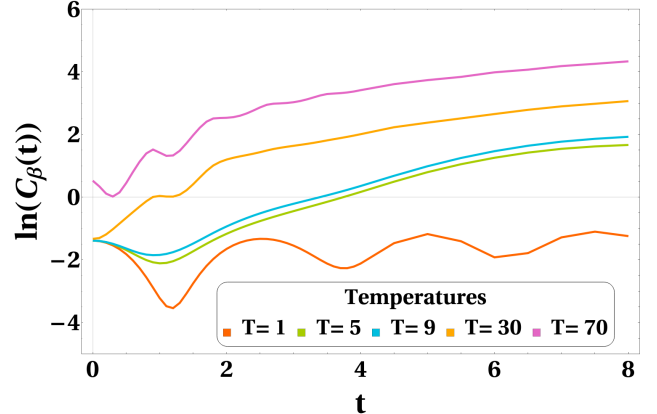


(b) Thermal OTOC

FIG. 13. OTOCs for *Model(II)* with $\sigma = 0.15$.

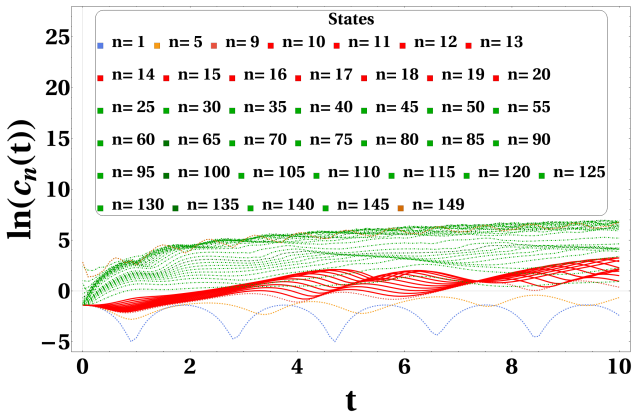


(a) Microcanonical OTOC

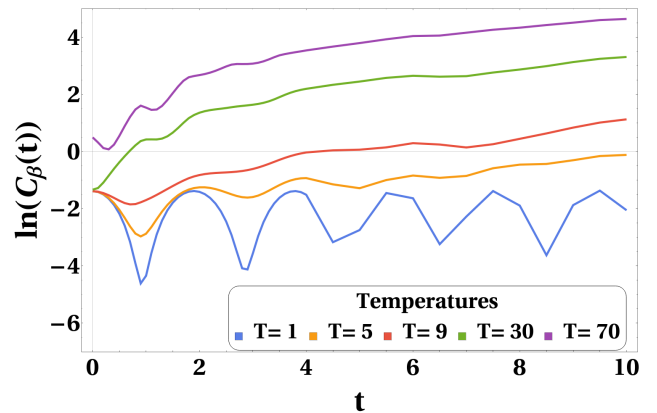


(b) Thermal OTOC

FIG. 14. OTOCs for *Model(II)*, $\sigma = 10.0$.

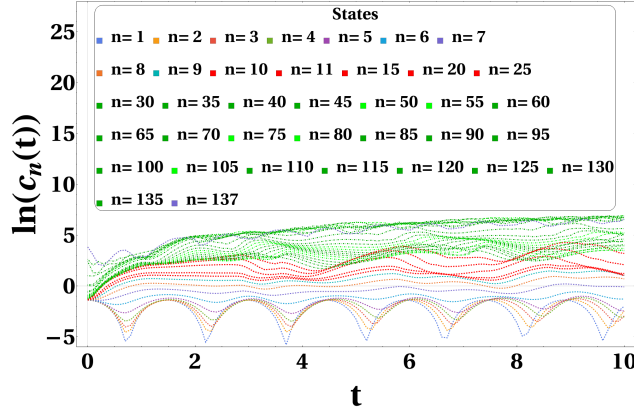


(a) Microcanonical OTOC

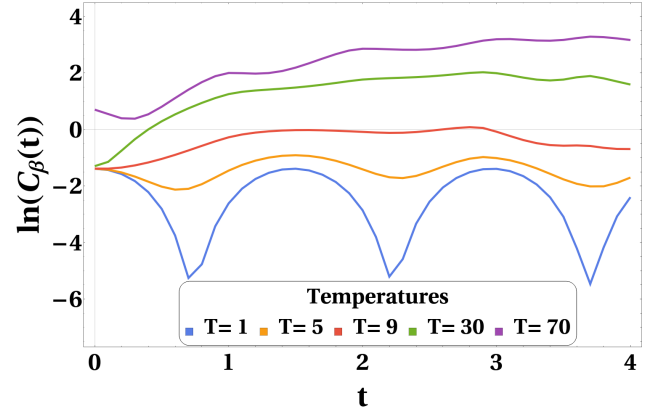


(b) Thermal OTOC

FIG. 15. OTOCs for *Model(II)*, $\sigma = 30.0$.



(a) Microcanonical OTOC



(b) Thermal OTOC

FIG. 16. OTOCs for *Model(II)* with $\sigma = 70.0$.

In Fig.(13) and Fig.(14), we find exponential growth of OTOCs around the hilltop of the potential for $\sigma = 0.15$ and 10 , respectively as verified previously. While in Fig.(5(c)), for $\sigma = 30.0$, the local maximum starts to disappear from the potential but, both microcanonical and thermal OTOCs continues to show exponential growth as we can find in Fig.(15). For $\sigma = 70$, in Fig.(6(d)), the local maximum is completely absent in the potential, but we can still find exponential growth for a very narrow band of energy levels in Fig.(16). Here, the time duration of exponential growth is very small compared to the rest.

If we compare the OTOCs of Model(I) and Model(II), then we will find that, the microcanonical OTOC for *Model(I)* shows a longer time exponential growth than the *Model(II)*. The exact same behaviour is also seen for thermal OTOC as well.

3. *Model(III)*

Then considering potential for *Model(III)*(Eq.(15)), we numerically plotted Eq.(6) and Eq.(5), for different values of σ in Fig.(17), Fig.(18).

In Fig.(17(a)) and Fig.(17(b)), we find exponential growth of Microcanonical OTOCs around the hilltop of the potential for $\sigma = 0.0$ and 0.15 , respectively as verified previously. Similarly, for higher temperature, thermal OTOC shows Exponential growth for the above mentioned σ values as show in Fig.(18(a)) and Fig.(18(b)). While in Fig.(6(c)), for $\sigma = 10.0$, the local maximum starts to disappear from the potential but, both microcanonical and thermal OTOCs continues to show exponential growth as we can find in Fig.(17(c)) and Fig.(18(c)). For $\sigma = 30$, in Fig.(6(d)), the local maximum is completely absent in the potential, but we can still find exponential growth for a very narrow band of energy levels in Fig.(17(d)) and Fig.(18(d)). Here, the time duration of exponential growth falls shorter than the previous of the σ values.

For computational purpose all calculations are done considering time-step 0.1.

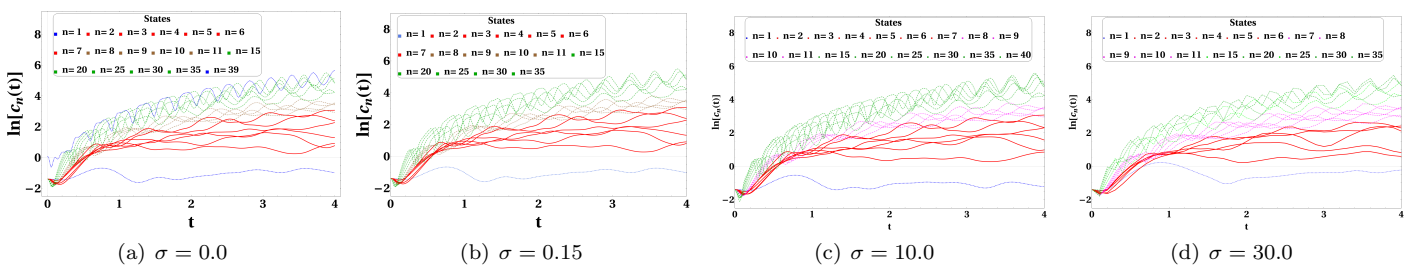


FIG. 17. Microcanonical OTOCs for *Model(III)*, at different values of σ .

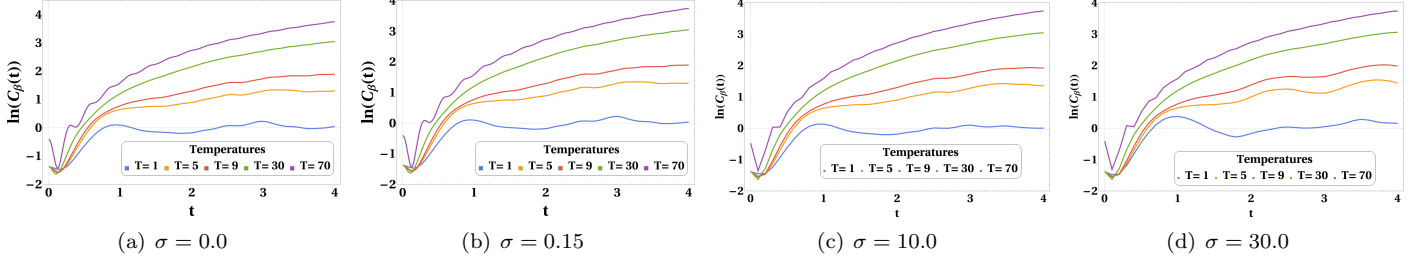


FIG. 18. Thermal OTOCs for *Model(III)* at different values of σ .

4. Model(IV)

Considering potential for *Model(IV)*(Eq.(16)), we numerically plotted Eq.(6) and Eq.(5), for different values of σ in Fig.(19) and Fig.(20).

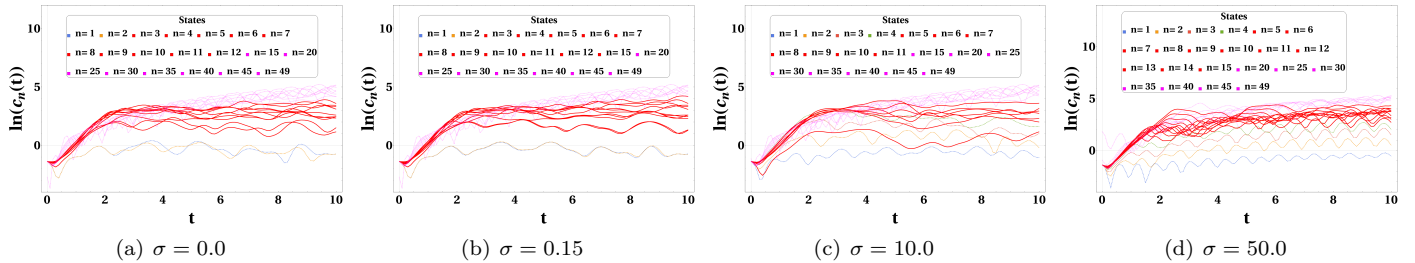


FIG. 19. Microcanonical OTOCs for *Model(IV)* with different values of σ .

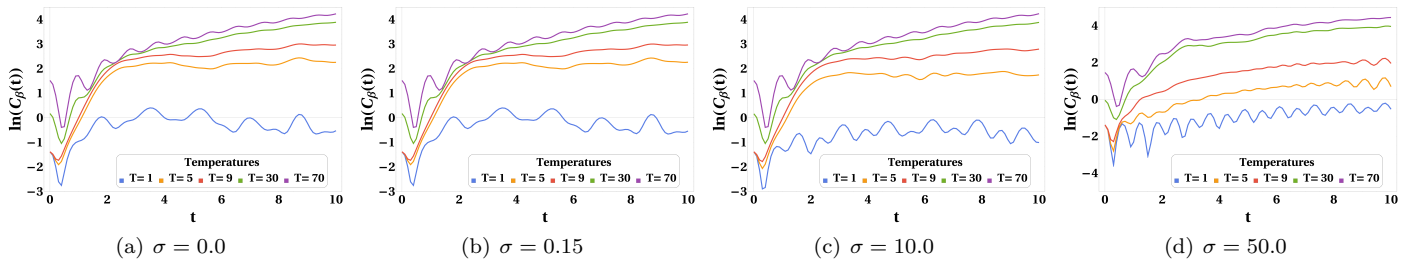


FIG. 20. Thermal OTOCs for *Model(IV)* with different values of σ .

Here we find that the microcanonical OTOC shows exponential growth near the plateau for $\sigma = 0.0$ and 0.15 in Fig.(19(a)) and in Fig.(19(b)) respectively. Similarly, the behaviour of thermal OTOC can be seen in Fig.(20(a)) and Fig.(20(b)) for the same value of σ s. However, for $\sigma = 10.0$, the plateau becomes a local maximum and for $\sigma = 50.0$, neither the plateau nor the local maximum is present as shown in Fig.(7(c)) and Fig.(7(d)). Nevertheless, at these asymmetry strengths, microcanonical OTOC continues to show exponential growth, as shown in Fig.(19(c)) and Fig.(19(d)). Thermal OTOC also shows exponential growth at these values for higher temperatures, as shown in Fig.(20(c)) and Fig.(20(d)).

IV. DISCUSSION

In specific classical systems, a small symmetry-breaking term in the Hamiltonian can lead to non-linear resonances in the regions where symmetry-breaking occurs. Chaos first appears in these regions, and as these regions grow, chaos also grows in the system making it more chaotic than before.

Here, we broke the symmetry present in the shape of the potential function by introducing a perturbation(Λx) to the Hamiltonian shown in Fig.(21) with the help of a symmetry-breaking term or an asymmetry parameter(σ). The effect of this perturbation with the growing strength of σ is corroborated by numerically observing the behaviour of 4-point OTOC, Loschmidt echo and SFF in the regions where symmetry breaking took place.

The presence of an unstable equilibrium engenders the exponential growth of OTOC in the neighbourhood of that equilibrium at an earlier time. This phenomenon was observed by many authors heretofore. However, our result showed that eradicating such an unstable equilibrium from the system by introducing perturbation(or breaking the existing

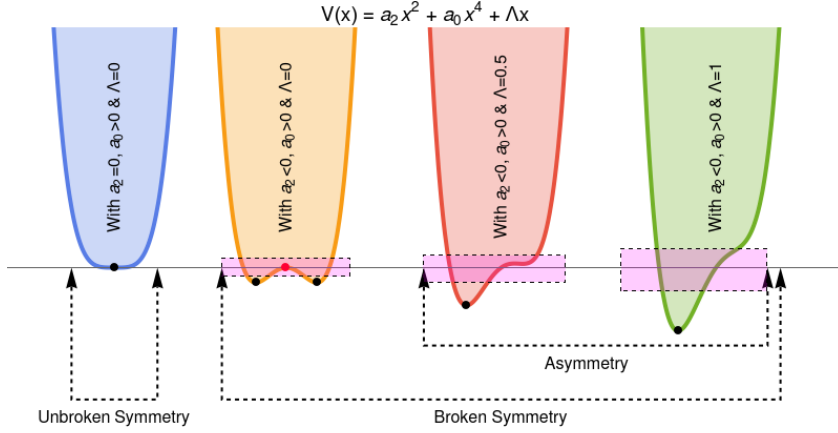


FIG. 21. Schematic diagram of a potential function, $V(x) = a_2x^2 + a_0x^4 + \Lambda x$, where by varying parameters(a_2 , a_0 & Λ) symmetry is spontaneously broken. For $a_2 = \Lambda = 0$ & $a_0 > 0$, we get a single well. For $a_2 < 0$, $a_0 > 0$ & $\Lambda = 0$, the existing symmetry of the single-well is broken and produces a double well which is a lower symmetric state. For $a_2 < 0$, $a_0 > 0$ & $\Lambda > 0$, the existing symmetry of the double-well is broken and the system ends up in asymmetric state. The minima and maxima are shown in black and red dots, respectively. And the broken-symmetric region is marked in magenta.

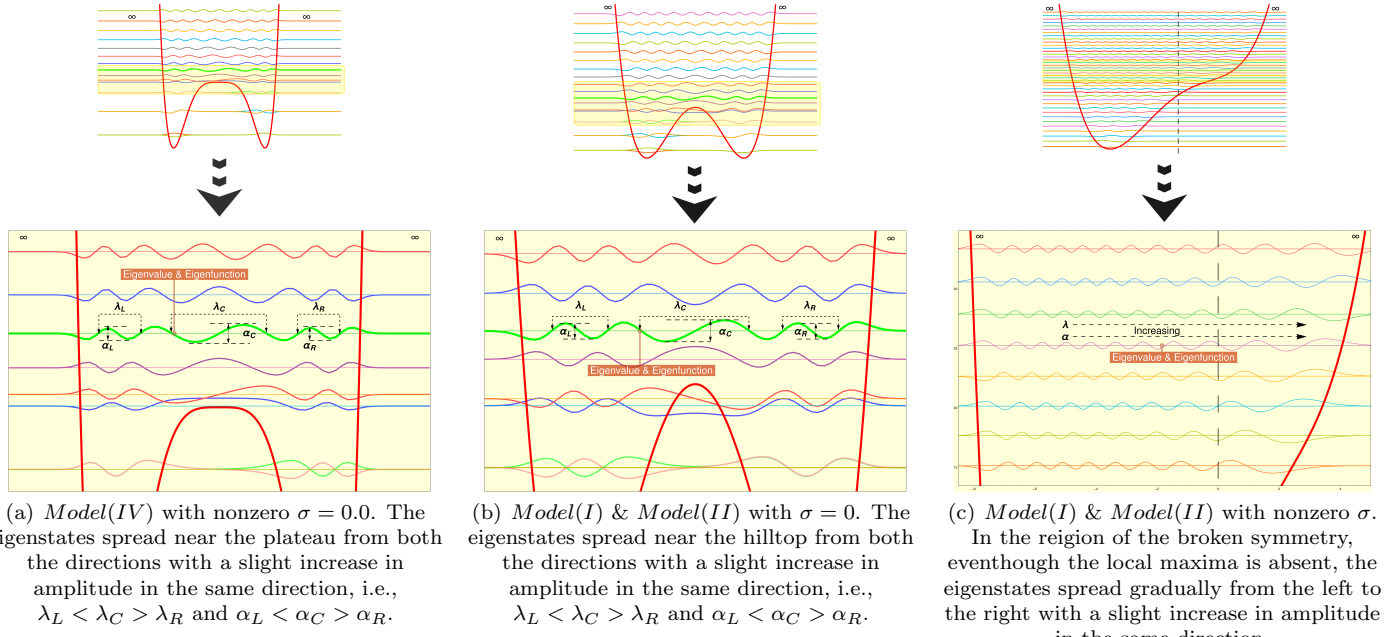


FIG. 22. Stretching of eigenstates because of symmetry breaking. λ and $\frac{\alpha}{2}$ are the wavelength and amplitude of the eigenstates, respectively.

symmetry in the potential) does not necessarily take the exponential growth of OTOC away from the system but rather pares the growth.

This happens because of the spontaneous symmetry-breaking of the Hamiltonian. As the symmetry breaks, asymmetry appears in potential function leading to the disappearance of degeneracy from the system. This ultimately leads to anomalies in the energy eigenfunctions in the neighbourhood of these broken-symmetric regions, shown in Fig.(22). The wavelength and the amplitude of the eigenfunctions on the right side have higher values than the left side of the potential. This symmetry-breaking effect can be seen for all four potentials mentioned above. Here, the four-point OTOC captures the irregularities in the eigenfunctions that have their origin in the symmetry breaking. In other words, the exponential growth of the four-point OTOC is broadly due to symmetry breaking in the potential rather than the presence of a local maximum. We have also observed that as the strength of perturbation increases, the broken symmetric regions widen. As a result, an extensive range of consecutive eigenstates show exponential growth but for shorter periods. As we move up in the potential wells, the energy values become sufficiently high and suppress the effect of symmetry breaking on the eigenfunctions. Hence the anomalies slowly disappear, making the results from four-point OTOC fall short. However, if we keep increasing the perturbation strength, the last term in the potential becomes dominant and drives the system. The system loses its originality and becomes a new one as a whole, which does not show the previously seen behaviour of OTOC any more.

Loschmidt Echo

The unperturbed Hamiltonian is

$$\mathcal{H}_1 = \frac{-i}{2} \nabla_x^2 + V(\hat{x}) \quad (17)$$

with $V(\hat{x}) = a_0 \hat{x}^4 - a_2 \hat{x}^2 - \eta$ for *Model(I)* and *Model(II)* and $V(\hat{x}) = a_2 \hat{x}^2 - a_0 \hat{x}^4 + \hat{x}^6 - \eta$ for *Model(III)*. Then the perturbed Hamiltonian is

$$\mathcal{H}_2 = \mathcal{H}_1 + \Lambda \hat{x} \quad (18)$$

where $\Lambda \hat{x}$ is the perturbation operator, defined as

$$\Lambda \hat{x} = H_2 - H_1 \quad (19)$$

where $\Lambda = \sigma \sqrt{\frac{a_0}{2a_2}}$ parametrises its strength. Here, we assume that $\Lambda \hat{x}$ is classically small but quantum mechanically significant such that the perturbation does not change the topology of the trajectories but introduces a phase difference.

TABLE II. Values of perturbation strength(Λ) for different values of asymmetry parameter(σ).

σ	Λ		
	<i>Model(I)</i> & <i>Model(II)</i>	<i>Model(III)</i>	<i>Model(IV)</i>
0.0	0.0	0.0	0.0
0.15	0.0188	0.0959	0.0229819
10.0	1.2500	6.3900	1.53214
30.0	3.7500	19.1703	-
50.0	-	-	7.66066
70.0	8.7500	-	-

Now, to compute Eq.(7), we follow the algorithm given by A. Peres in [21]. It follows that

$$\begin{aligned} M(t) &= \left| \langle \Psi_0 | e^{i(\hat{H}_2 - \hat{H}_1)t/\hbar} | \Psi_0 \rangle \right|^2 \\ &= \left| \langle \Psi_0 | e^{i\Lambda \hat{x} t/\hbar} | \Psi_0 \rangle \right|^2 \\ &= \left| \langle \Psi_0 | e^{i\hat{x}\tau} | \Psi_0 \rangle \right|^2 \end{aligned} \quad (20)$$

where $\tau = \frac{\Lambda t}{\hbar}$

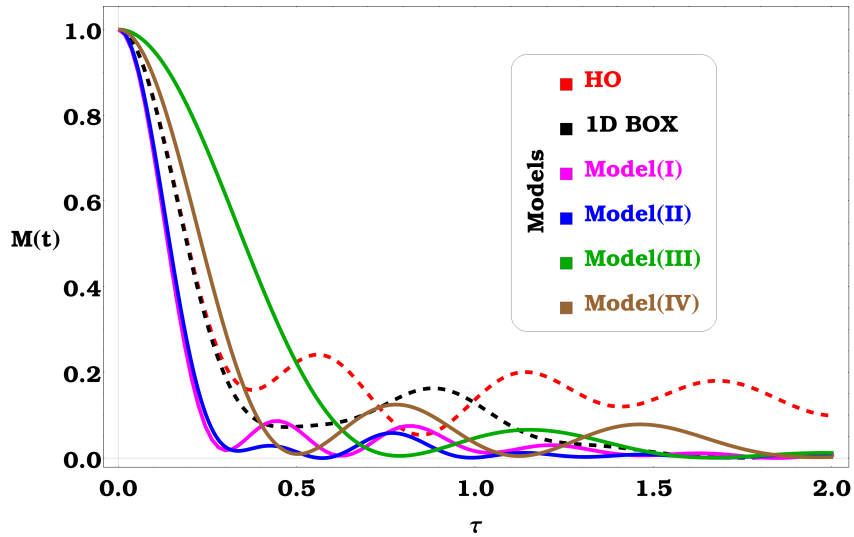


FIG. 23. Loschmidt Echo of Harmonic Oscillator(HO) (red dashed line), One Dimensional Box(1D Box) (black dashed lines), *Model(I)* (magenta), *Model(II)* (blue), *Model(III)* (green) and *Model(IV)* (brown).

For different values of Λ (perturbation strengths), given in Table(II), we numerically observe that LE decays exponentially for a very short time and then shows small amplitude oscillations as expected. The collage of LEs for Harmonic

Oscillator(HO), 1D Box, *Model(I)*, *Model(II)* and *Model(IV)* is shown in Fig.(23). After initial exponential decay, the LE fluctuates with high amplitude for HO and 1D box and for our systems, the fluctuations are small indicating anomalies.

Spectral Form Factor

Another quantity related to OTOC and Loschmidt Echo is the spectral form factor(SFF) [22–24]. In a chaotic system, the SFF exhibits a dip-ramp-plateau structure, while the ramp is not present in integrable systems. To alleviate the computation and to achieve more physical intuition, with the analytical continuance, the partition function can be defined as

$$\mathcal{Z}(\beta, t) = Z(\beta + it) = \text{Tr}(e^{-\beta\mathcal{H}-i\mathcal{H}t}) \quad (21)$$

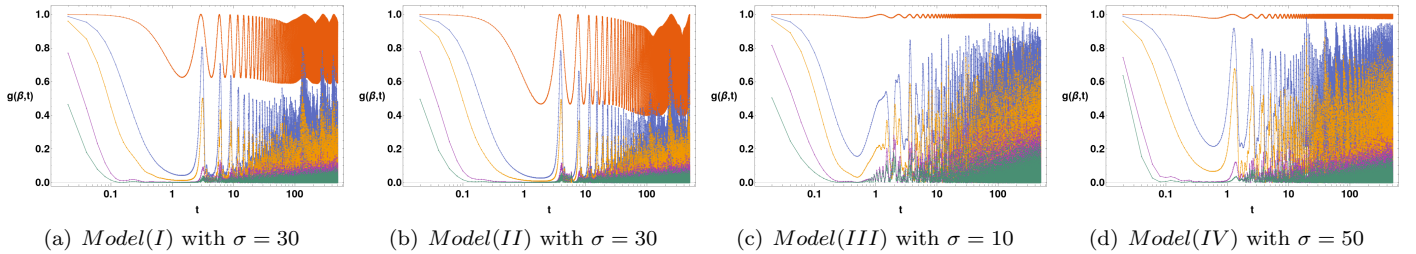


FIG. 24. SFF as a function of time for five different temperatures $T = 1$ (orange), 5 (blue), 9 (yellow), 30 (purple) and 70 (green).

where \mathcal{Z} is the partition function, β is inverse temperature, otherwise known as the "coldness function", and t is time. We have continued β to $\beta + it$. The time average of $\mathcal{Z}(\beta, t)$ vanishes, so it is an oscillating function around zero.

Normalizing it by the partition function, we can determine the size of fluctuations:

$$g(\beta, t) = \left| \frac{\mathcal{Z}(\beta, t)}{Z(\beta)} \right|^2 = \frac{1}{|Z(\beta)|^2} \sum_{m,n} e^{-\beta(E_m+E_n)} e^{i(E_m-E_n)t} \quad (22)$$

The function $g(\beta, t)$ is the desired SFF.

The SFFs for all three models are shown in Fig.(24). At low temperatures, $g(\beta, t)$ seems first to decrease and then bounce back to its value at early times, while for high temperatures, $g(\beta, t)$ first drops, then rises, followed by a plateau with intense fluctuations. The high-temperature behaviour of $g(\beta, t)$ is not very dissimilar from that of a single random matrix.

V. CONCLUSION

The exponential growth of both microcanonical and thermal OTOC in the neighbourhood of the local maximum of an IHO potential is a well-known fact; however, it is incomplete. With several examples, we demonstrate that even without a local maximum, OTOC shows exponential growth in the same neighbourhood, and in some cases, this region broadens. Hence, the cause of this growth, in general, cannot be due to the presence of a local maximum but due to the spontaneous symmetry breaking in the Hamiltonian. The behaviour of OTOC in a single-well potential is periodic. However, by varying an order parameter, when we break the existing symmetry in the Hamiltonian of this system, it ends up with one local maximum and two minima (*Model(I)* and *Model(II)*) or two maxima and three minima (*Model(III)*) or a plateau and two minima (*Model(IV)*). Irrespective of their shapes, early time exponential growth of OTOC comes into the picture in the neighbourhood of the broken symmetric regions, which happens to be around the local maxima of these wells. When we further break the symmetries and make the systems free of any local maximum, even then, OTOC continues to show exponential growth in a broader region, although for a shorter time, in the regions where symmetry breakings occur. Chaos first appears in the neighbourhood of the broken symmetric regions, and as the parameter responsible for it strengthens, the chaotic regions also expand. Here OTOC, a quantum mechanical diagnostic tool for chaos, beautifully captures the effects of symmetry-breaking, although the models under study are regular integrable systems. Therefore, our study provides compelling evidence supporting the importance of symmetry breaking when analysing the behaviour of complex quantum mechanical systems, which has important implications for understanding various physical systems, from condensed matter systems to black holes.

Overall, the study of OTOCs and symmetry breaking has important implications for our understanding of quantum chaos and the behaviour of complex systems. We aim to extend our research further into the matter considering coupled

- [1] N. Anand, G. Styliaris, M. Kumari, and P. Zanardi, “Quantum coherence as a signature of chaos,” *Phys. Rev. Research*, vol. 3, p. 023214, Jun 2021. [2](#)
- [2] K. Hashimoto, K. Murata, and R. Yoshii, “Out-of-time-order correlators in quantum mechanics,” *Journal of High Energy Physics*, vol. 2017, p. 138, Oct 2017. [3](#)
- [3] K. Hashimoto, K.-B. Huh, K.-Y. Kim, and R. Watanabe, “Exponential growth of out-of-time-order correlator without chaos: inverted harmonic oscillator,” *Journal of High Energy Physics*, vol. 2020, p. 68, Nov 2020. [3](#), [7](#)
- [4] K. Y. Bhagat, B. Bose, S. Choudhury, S. Chowdhury, R. N. Das, S. G. Dastider, N. Gupta, A. Maji, G. D. Pasquino, and S. Paul, “The generalized otoc from supersymmetric quantum mechanics—study of random fluctuations from eigenstate representation of correlation functions,” *Symmetry*, vol. 13, no. 1, 2021. [3](#)
- [5] W. Kirkby, D. H. J. O’Dell, and J. Mumford, “False signals of chaos from quantum probes,” *Phys. Rev. A*, vol. 104, p. 043308, Oct 2021. [3](#)
- [6] N. Aquino, J. Garza, G. Campoy, and A. Vela, “Energy eigenvalues for free and confined triple-well potentials,” *Revista Mexicana De Fisica*, vol. 57, pp. 46–52, 2011. [4](#), [6](#)
- [7] S. Gentilini, M. C. Braidotti, G. Marcucci, E. DelRe, and C. Conti, “Physical realization of the glauber quantum oscillator,” *Scientific Reports*, vol. 5, p. 15816, Nov 2015. [4](#)
- [8] V. Subramanyan, S. S. Hegde, S. Vishveshwara, and B. Bradlyn, “Physics of the inverted harmonic oscillator: From the lowest landau level to event horizons,” *Annals of Physics*, vol. 435, p. 168470, 2021. Special issue on Philip W. Anderson.
- [9] S. Choudhury, S. P. Selvam, and K. Shirish, “Circuit complexity from supersymmetric quantum field theory with morse function,” *Symmetry*, vol. 14, p. 1656, aug 2022. [4](#)
- [10] M. V. Berry and J. P. Keating, “The riemann zeros and eigenvalue asymptotics,” *SIAM Review*, vol. 41, no. 2, pp. 236–266, 1999. [4](#)
- [11] T. Morita, “Thermal emission from semiclassical dynamical systems,” *Phys. Rev. Lett.*, vol. 122, p. 101603, Mar 2019. [4](#)
- [12] L. Reichl, *The Transition to Chaos: Conservative Classical and Quantum Systems*. Fundamental Theories of Physics, Springer International Publishing, 2021. [5](#)
- [13] V. I. Kuvshinov, A. V. Kuzmin, and V. A. Piatrou, “Asymmetric double well system as effective model for the kicked one,” 2011. [5](#)
- [14] R. P. McRae and B. C. Garrett, “Anharmonic corrections to variational transition state theory calculations of rate constants for a model activated reaction in solution,” *The Journal of Chemical Physics*, vol. 98, pp. 6929–6934, 05 1993.
- [15] A. J. Brizard and M. C. Westland, “Motion in an asymmetric double well,” *Communications in Nonlinear Science and Numerical Simulation*, vol. 43, pp. 351–368, 2017.
- [16] M. Selg, “Exactly solvable asymmetric double-well potentials,” *Physica Scripta*, vol. 62, p. 108, aug 2000. [5](#)
- [17] K. Wittmann W., E. R. Castro, A. Foerster, and L. F. Santos, “Interacting bosons in a triple well: Preface of many-body quantum chaos,” *Phys. Rev. E*, vol. 105, p. 034204, Mar 2022. [6](#)
- [18] R. J. Damburg, R. K. Propin, and Y. I. Ryabykh, “Perturbation theory for the triple-well anharmonic oscillator,” *Phys. Rev. A*, vol. 41, pp. 1218–1224, Feb 1990. [6](#)
- [19] T. Morita, “Extracting classical lyapunov exponent from one-dimensional quantum mechanics,” *Phys. Rev. D*, vol. 106, p. 106001, Nov 2022. [7](#)
- [20] P. Garbaczewski, V. A. Stephanovich, and G. Engel, “Electron spectra in double quantum wells of different shapes,” *New Journal of Physics*, vol. 24, p. 033052, mar 2022. [7](#)
- [21] A. Peres, “Stability of quantum motion in chaotic and regular systems,” *Phys. Rev. A*, vol. 30, pp. 1610–1615, Oct 1984. [14](#)
- [22] R. de Mello Koch, J.-H. Huang, C.-T. Ma, and H. J. Van Zyl, “Spectral form factor as an otoc averaged over the heisenberg group,” *Physics Letters B*, vol. 795, pp. 183–187, 2019. [15](#)
- [23] Z. Cao, Z. Xu, and A. del Campo, “Probing quantum chaos in multipartite systems,” *Phys. Rev. Res.*, vol. 4, p. 033093, Aug 2022.
- [24] P. Romatschke, “Quantum mechanical out-of-time-ordered-correlators for the anharmonic (quartic) oscillator,” *Journal of High Energy Physics*, vol. 2021, p. 30, Jan 2021. [15](#)